Applied Ocean Research 125 (2022) 103250

Contents lists available at ScienceDirect

Applied Ocean Research

journal homepage: www.elsevier.com/locate/apor

Parameterised transfer functions with associated confidence bands

Ulrik D. Nielsen [a,b,*], Raphaël E.G. Mounet [a,b], Astrid H. Brodtkorb [b]

[a] DTU Mechanical Engineering, Technical University of Denmark, DK-2800 Kgs. Lyngby, Denmark
[b] Centre for Autonomous Marine Operations and Systems, NTNU AMOS, NO-7052 Trondheim, Norway

ARTICLE INFO

Keywords:
Parameterised transfer functions
Directional wave spectrum
Ship motion prediction
Confidence bands
Uncertainty estimation

ABSTRACT

This paper presents a method that can be used to obtain the motion transfer functions of a ship when the detailed hull geometry is not available. In the method, any parameterised transfer function can be optimised from a data-driven approach that compares a measured response spectrum and the corresponding theoretical spectrum based on the combination of transfer function and wave spectrum. The established method facilitates association of 95% confidence bands which are useful to indicate a level of trust. The proposed method is evaluated on a conceptual level using both simulated and in-service measurements, and promising results are obtained.

1. Introduction

The seakeeping performance of ships is often evaluated by use of transfer functions, describing how waves translate into motions and other derived responses for a given frequency (or wave length) and wave encounter angle. In general, transfer functions are estimated from the knowledge of the ship geometry, and additionally they depend on the loading condition and forward speed. They can be computed by solving the equations of motions for the ship, often on the basis of potential flow theory by formulating radiation-diffraction codes via 3D panel methods or strip theory (Salvesen et al., 1970), typically with little, if any, degradation in accuracy by application of strip theory (Parunov et al., 2022). Notwithstanding, in either case, the details of the geometry are required which means that the hull lines must be available. However, in early stages of ship design projects, the lines are not available and, in case of existing, in-service ships, the hull lines are not necessarily to the disposition of the ship operator or, say, third-party performance optimisation companies. With this argument, the tuning of semi-analytical transfer functions, so-called closed-form expressions (Jensen et al., 2004), was proposed by Nielsen et al. (2021), noticing that the closed-form expressions take as basic input only the main dimensions (length, breadth, draught) of the ship. In the method, a correction coefficient was established through spectral analysis, thus leading to a correction coefficient explicitly depending on wave frequency and encounter angle for given operational conditions (draught, forward speed, etc.). It was shown that the use of the correction coefficient could improve predictions of the particular response that was initially "tuned". One concern, however, evident from the application to data, was a nonphysical saw-toothed behaviour considering the correction coefficient's variation with frequency, also observed by Mounet et al. (2022b). This spurious behaviour can be mitigated to some extent by averaging over appropriately large amounts of data/samples via elaborate postprocessing, compromising the very idea to have a simple and practical method offering reliable response predictions based on semi-analytical, closed-form transfer functions.

1.1. Scope and novelty

The present study continues along the lines of Nielsen et al. (2021), but herein it is suggested to optimise directly the governing parameters of the closed-form transfer functions developed by Jensen et al. (2004). In the original work, the set of closed-form expressions apply to a box-shaped vessel, and the ship's physical counterparts of length (L_{pp}), breadth (B), draught (T), etc. constitute the fundamental input parameters. Qualitatively, the closed-form transfer functions prescribe the wave-induced motions in reasonable agreement with linear strip theory (Jensen et al., 2004), but quantitatively they are not necessarily a good match in their original form, as the transfer functions' amplitude drops to zero too early when comparing to potential flow codes (Mounet et al., 2022a; Nielsen et al., 2021). Rather than relying on the true physical dimensions of the ship, this study considers the parameterised transfer functions (Jensen et al., 2004) to depend on a set of parameters with no (true) physical resemblance considering the real ship. Thus, the values of the basic input parameters are computed from an optimisation established from spectral analysis equating the measured response spectrum with the corresponding theoretical spectrum, in a manner similar to the earlier study (Nielsen et al., 2021). It is

* Corresponding author at: DTU Mechanical Engineering, Technical University of Denmark, DK-2800 Kgs. Lyngby, Denmark.
E-mail address: udn@mek.dtu.dk (U.D. Nielsen).

https://doi.org/10.1016/j.apor.2022.103250
Received 15 February 2022; Received in revised form 22 April 2022; Accepted 13 June 2022

believed, however, that the present study carries the inherent simplicity all the way through, also in the postprocessing. In addition, the study proposes the inclusion of the 95% confidence bands on the computed transfer functions.

1.2. Composition

In addition to the introduction, the paper contains five sections: Section 2 outlines the necessary theory and explains the methodology used in the study. Section 3 presents the first set of results obtained from a case study considering simulated data, whereas Section 4 shows the potential of the developed method when it is applied to full-scale, in-service data. The two sections dealing with the results include specific discussions, while more general discussions and suggested further work are presented in Section 5. Finally, Section 6 makes concluding remarks.

2. Theory and methodology

2.1. Basic information and fundamental assumptions

The experienced seaway is the result of a short-crested wave system, and resulting processes are assumed to be stationary and ergodic. Although changing environmental and operational conditions compromise this assumption, a limitation to, say, 30 min time windows means that the assumption can be met for many practical purposes.

The directional wave spectrum $E(\omega_0, \mu)$ fully characterises the energy density of the wave system; ω_0 is the circular wave frequency [rad/s] and μ [deg] is the direction where the energy comes from. The index $_0$ on ω_0 is used to emphasise that the wave spectrum is a function of the intrinsic, and *absolute*, frequency. In the analysis of in-service data (Section 4), the directional wave spectra obtained from the ERA5 database (Hersbach et al., 2021) are used, but, in principle, 2D wave spectra obtained from any available source could be considered; obviously with the requirement that the source must be reliable both in terms of accuracy and in terms of availability and accessibility at the actual geographical position, in time and space, of the studied ship.

In principle, any global wave-induced ship response R can be considered; for instance, one of the 6 DOF motion components. The corresponding transfer function is $\Phi_R(\omega_0, \beta)$; β [deg] is wave encounter angle, i.e. the angle between the direction of the incident wave and the ship's longitudinal axis where $\beta = 180$ deg corresponds to head sea. Onwards, β will also be termed the *relative wave direction*. The transfer function depends implicitly on operational parameters such as the ship's forward speed U and the loading condition represented by draught T.

Various numerical methods (closed-form expressions, strip theory, 3D panel codes, ...) can be used to compute estimates of transfer functions, noticing that irrespectively of the method, the use of transfer functions assumes a linear relationship between waves and the induced responses.

2.2. Parameterised transfer functions

In this study, the closed-form transfer functions derived by Jensen et al. (2004) are considered; noticing that herein they are referred to by *parameterised transfer functions*, in many cases simply abbreviated PTF. In the original work, heave, pitch, and roll are studied, but the present work focuses on pitch exclusively although the developed method is generic and can easily be applied to the other responses. The following derivation is comparable to the original study (Jensen et al., 2004) and is included here to illustrate how the transfer function of pitch is parameterised. Note that, in a complete and general form, transfer functions are complex-valued, or equivalently with two parts being the modulus and the argument. Jensen et al. (2004) considers only the "frequency response function", i.e. the modulus of the transfer function, but (Mansour et al., 2004) derive also the argument for some of the responses although this is not studied in the following.

2.2.1. Modulus of pitch

The ship hull is approximated by a rectangular box with dimensions $L \times B \times T$ for length, breadth, and draught, respectively; hence, there is no coupling between heave and pitch. The equation of motion for pitch θ is,

$$2\frac{k_w T}{\omega_0^2}\ddot{\theta} + \frac{A^2}{k_w B \alpha^3 \omega_0}\dot{\theta} + \theta = aG\sin(\omega_e t) \tag{1}$$

Here a is the wave amplitude, $k_w = \frac{\omega_0^2}{g}$ is the wave number, assuming deep water, g is the acceleration of gravity, and t is time. Differentiation with respect to time is denoted by a dot. The Doppler shift is introduced through the parameter α defined by,

$$\alpha = 1 - F_n\sqrt{k_w L}\cos\beta \tag{2}$$

and thus $\omega_e = \alpha\omega_0$ is the frequency of encounter, where the Froude number $F_n = U/\sqrt{gL}$.

The shape effect of the hull geometry is accounted for alone by the block coefficient C_b. It can be included most appropriately by simply taking the breadth as:

$$B = B_0 C_b \tag{3}$$

where B_0 is the maximum waterline breadth. Thus, the ship is represented by a homogeneously loaded box-shaped barge with the beam modified so that the total mass of the ship equals the buoyancy of the ship.

In the following, note that all parameters depend explicitly on the absolute frequency ω_0 introduced via the Doppler shift, although this is not necessarily specified.

The sectional hydrodynamic damping A is modelled by the dimensionless ratio between the incoming and the diffracted wave amplitudes through the following approximation, Yamamoto et al. (1986):

$$A = 2\sin\left(\frac{1}{2}k_w B\alpha^2\right)\exp(-k_w T\alpha^2) \tag{4}$$

The forcing function G is given by,

$$G = \kappa f \frac{24}{(k_e L)^2 L}\left(\sin\left(\frac{k_e L}{2}\right) - \frac{k_e L}{2}\cos\left(\frac{k_e L}{2}\right)\right) \tag{5}$$

where

$$k_e = |k_w\cos\beta| \tag{6}$$

$$f = \sqrt{(1 - k_w T)^2 + \left(\frac{A^2}{k_w B\alpha^3}\right)^2} \tag{7}$$

The Smith correction factor κ is approximated by

$$\kappa = \exp(-k_w T) \tag{8}$$

Finally, the solution to Eq. (1), in terms of the modulus of the pitch transfer functions, is

$$\Phi_\theta(\omega_0) = \eta|G| \tag{9}$$

where

$$\eta = C_1\left(\sqrt{\left(1 - 2k_w T\alpha^2\right)^2 + \left(\frac{A^2}{k_w B\alpha^2}\right)^2}\right)^{-1} \tag{10}$$

emphasising that the factor C_1 is introduced exclusively in the present study, as the factor does not appear in the original formulas (Jensen et al., 2004).

It is realised that the forcing function of pitch, and thus pitch itself, approaches zero when the encounter angle between ship and waves becomes 90 deg, equivalently 270 deg, in line with the hydrodynamics of a box-shaped vessel. In reality, normal ships do not have fore-aft symmetry and, although little, pitching will occur while sailing in (long-crested) beam waves. In contrast to the original work (Jensen

et al., 2004), this has been accounted for in the present study by assuming

$$\Phi_\theta(\omega_0|\beta = 90 \text{ deg}) = \Phi_\theta(\omega_0|\beta = 270 \text{ deg}) \equiv 0.1 \cdot \Phi_\theta(\omega_0|\beta = 80 \text{ deg}) \quad (11)$$

The value 0.1 is reflecting a somewhat arbitrary choice, as the point is that, while the pitch transfer function is small for heading 90 deg., it is *not* zero. The exact value is not so important, as an optimisation will be performed anyway.

2.3. Spectral analysis

From measurements of the response R, the response spectrum can be estimated as $\widetilde{S}_R(\omega_e)$; for instance, it can be computed by FFT or similar methods. Note that the (encountered) spectrum is an explicit function of the encounter frequency ω_e [rad/s]. A theoretical estimate $\widehat{S}_R(\omega_e)$ of the response spectrum can be obtained by the combined use of the wave spectrum and the transfer function of the given response in question. In this case,

$$\widehat{S}_R(\omega_e) = \int_0^{2\pi} |\Phi_R(\omega_e, \beta)|^2 E_e(\omega_e, \mu) d\mu \quad (12)$$

$$\beta = 180 - (\chi - \mu) \quad (13)$$

$$\omega_e = \omega_0 - \omega_0^2 \psi, \;\; \psi = \frac{U}{g}\cos\beta \quad (14)$$

$$E_e(\omega_e, \mu) = \left\langle E(\omega_0, \mu)\frac{d\omega_0}{d\omega_e}\right\rangle_{\omega_e} \quad (15)$$

$$\Phi_R(\omega_e, \beta) = \langle \Phi_R(\omega_0, \beta)\rangle_{\omega_e} \quad (16)$$

$$\varepsilon(\omega_e) = \widetilde{S}_R(\omega_e) - \widehat{S}_R(\omega_e) \quad (17)$$

where χ is the compass heading of the ship. The frequency conversion introduced in Eqs. (15) and (16) via Eq. (14) is necessary since the wave spectrum per se is given as a function of the intrinsic, and thus absolute, frequency ω_0. For the same reason, the straight-line brackets $\langle\cdots\rangle_{\omega_e}$ with ω_e as index is used to emphasise that evaluation happens for a given frequency of encounter ω_e; this is discussed in more details below. The error $\varepsilon(\omega_e)$ between the theoretical estimate $\widehat{S}_R(\omega_e)$ and the measured response spectrum $\widetilde{S}_R(\omega_e)$ is assumed to be normally distributed. Note also that, in general, the ship's compass course and heading (= orientation of longitudinal axis) are different but herein they are assumed identical, since no side-way drift is assumed.

In Section 2.2, the parameterised transfer function of pitch was outlined. Similar expressions exist for other motion components (Jensen et al., 2004) and, generally, the transfer functions depend on a set of parameters, such as L (length), B (breadth), T (draught), that can be organised in a vector $\mathbf{Y}$. Hence,

$$\Phi_R(\omega_0, \beta) \equiv \Phi_R(\omega_0, \beta|\mathbf{Y}) \quad (18)$$

Strictly speaking, the vector, say, $\mathbf{Y} = [L, B, T, C_1]$ is fixed when a specific ship in a particular operational scenario is given since, in the original derivation (Jensen et al., 2004), the parameters all represent physical quantities describing the actual ship in question. On the other hand, this viewpoint can be relaxed by simply assuming the parameters to be "fitting parameters" without any (true) physical meaning. In this case, the parameters in $\mathbf{Y}$ can be optimised by minimising the error $\varepsilon(\omega_e)$, cf. Eq. (17). Thus, consideration of the entire range of relevant encounter frequencies leads to the following nonlinear problem with least squares objective function,

$$\min_{\mathbf{Y}} \sum_{j=1}^{J} \left| \widetilde{S}_R(\omega_{e,j}) - \int_0^{2\pi} \left\langle |\Phi_R(\omega_0, \beta|\mathbf{Y})|^2 E(\omega_0, \mu)\frac{d\omega_0}{d\omega_e}\right\rangle_{\omega_{e,j}} d\mu \right|^2 \quad (19)$$

It is noted that the interval of encounter frequencies is discretised as $\{\omega_{e,1}, \omega_{e,2}, \ldots, \omega_{e,J}\}$, and emphasising that the integrand must be computed for given ω_e, as introduced above and further outlined in the following.

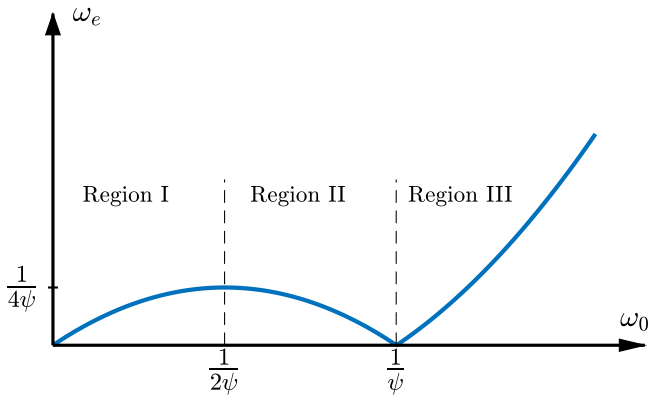

$$\text{Region I:} \quad \omega_{0,1} = \frac{1 - \sqrt{1 - 4\psi\omega_e}}{2\psi}$$

$$\text{Region II:} \quad \omega_{0,2} = \frac{1 + \sqrt{1 - 4\psi\omega_e}}{2\psi}$$

$$\text{Region III:} \quad \omega_{0,3} = \frac{1 + \sqrt{1 + 4\psi\omega_e}}{2\psi}$$

Fig. 1. The relationship between the encountered frequencies and the absolute (wave) frequencies is governed by the Doppler Shift. If ω_0 is expressed in terms of ω_e, three solutions exist when the ship is in following sea *and* $\omega_e < \frac{1}{4\psi}$. This is indicated with indices 1, 2, and 3. Note that $\psi = U/g\cos\beta$.

2.3.1. Mapping between absolute and encounter domain

When a ship sails with non-zero forward speed relative to propagating waves, the mapping between the two frequency domains, absolute domain vs. encounter domain, is controlled by the Doppler shift as given by Eq. (14). In head sea conditions with 90 deg $\le \beta \le$ 270 deg, this is trivial. On the other hand, in following seas with $\beta <$ 90 deg and $\beta >$ 270 deg, and for non-zero forward speed, a given ω_e can be the result of up to three absolute frequencies. This is shown in Fig. 1, which is a graphical illustration of the Doppler shift for the particular condition of following sea and non-zero forward speed. It is recognised that if, and only if, $\omega_e > \frac{1}{4\psi}$ there is a 1-to −1 relationship between the encountered and the absolute frequency; otherwise there is a 1-to −3 relationship. Mathematically, the triple-valued relationship is an elementary fact that must hold in the response spectrum estimation in Eq. (12). In practical computations, this is rather delicate (Beck et al., 1989; Lindgren et al., 1999; Nielsen, 2017, 2018), but in a situation where the wave spectrum is known/given, like considered herein, the solution to the problem at hand is unique after all, in contrast to the case when the wave spectrum is unknown and is sought through an inverse problem (Iseki and Ohtsu, 2000; Nielsen, 2006).

The physical inference from Fig. 1 is that three distinct energy densities from the wave spectrum at $\omega_{0,1}$, $\omega_{0,2}$, and $\omega_{0,3}$ contribute to the encounter-response spectrum at ω_e, when a ship sails in following sea if $\omega_e < \frac{1}{4\psi}$. In general, for any given ω_e and following sea, the theoretical response spectrum should therefore be computed by,

$$\widehat{S}_R(\omega_e) = \begin{cases} \sum_{i=1}^{3} \left[\int_0^{2\pi} \left\langle |\Phi_R(\omega_{0,i}, \beta|\mathbf{Y})|^2 E(\omega_{0,i}, \mu)\frac{d\omega_{0,i}}{d\omega_e}\right\rangle_{\omega_e} d\mu \right], & \omega_e < \frac{1}{4\psi} \\ \sum_{i=2}^{3} \left[\int_0^{2\pi} \left\langle |\Phi_R(\omega_{0,i}, \beta|\mathbf{Y})|^2 E(\omega_{0,i}, \mu)\frac{d\omega_{0,i}}{d\omega_e}\right\rangle_{\omega_e} d\mu \right], & \omega_e = \frac{1}{4\psi} \\ \int_0^{2\pi} \left\langle |\Phi_R(\omega_{0,3}, \beta|\mathbf{Y})|^2 E(\omega_{0,3}, \mu)\frac{d\omega_{0,3}}{d\omega_e}\right\rangle_{\omega_e} d\mu, & \omega_e > \frac{1}{4\psi} \end{cases} \quad (20)$$

underlining again that the straight-line brackets with ω_e as index indicate that the integrand must be computed for given ω_e. The result shows

how to map frequency components of a theoretical response spectrum in the encounter domain. The central point about the mapping in Eq. (20) is to allow a comparison with a *measured* response spectrum, cf. Eqs. (12) and (19). On the other hand, from a theoretical point of view, it could be a choice to map the other way; that is, rather than mapping the theoretical response spectrum to the encounter domain, the measured spectrum could, in principle, be mapped to the absolute domain. In this case, however, the measured spectrum becomes heavily distorted and, from a practical point of view, the computational complications increase (Beck et al., 1989; Nielsen, 2017). The details of the mapping from absolute domain to encounter domain of the theoretical response spectrum are not dealt with any further herein, but it is noteworthy that the details are illustrated by Nielsen et al. (2021) via a pseudo code for the calculation of Eq. (20).

2.4. Optimisation of parameters

2.4.1. Sample-specific optimisation

The measured response spectrum $\widetilde{S}_R(\omega_e)$ corresponding to a time series sequence of length, say, 30 min is considered, and this constitutes a sample. The prerequisite for the optimisation of $\mathbf{Y}$ corresponding to the considered sample is the availability of the (ground true) wave spectrum. On a sidenote it should be mentioned that a conceptual study has been made by Mounet et al. (2022b) in which multiple, geographically-adjacent ships are considered simultaneously as introduced and discussed by, e.g., Nielsen et al. (2019) and Long et al. (2019). Although the particular research and applications are still in a developing phase, potentially, such a situation considering multiple ships can be used to combine sea state estimation and transfer function calibration via a leave-one-out principle (Mounet et al., 2022b).

It has been seen, cf. Section 2.2, that the combined effects of mass, damping, restoring, and excitation in the parameterised transfer function of pitch are controlled solely by the ship main dimensions length L, breadth B, draught T, and the introduced scaling factor C_1. In other words, all of these parameters have the ability to manipulate the shape of the transfer function, and consequently they should all be elements in the vector $\mathbf{Y}$ to optimise.

The very set of parameter values leading to the minimisation of Eq. (19) is denoted by $\mathbf{Y}^*$, and this set forms the solution of the *sample-specific* optimisation. It should be noticed that a reasonable starting guess of the minimisation of Eq. (19) is expected to be the values of $\mathbf{Y}$ equal to the values of the physical counterparts (length, breadth, draught, etc.) of the real ship. The practical implementation of the optimisation is made in MATLAB® using the function `fmincon` that can be applied to find the minimum of constrained nonlinear multivariable functions. The constraints are imposed by specifying bounds on the parameters in $\mathbf{Y}$. Later, additional remarks are given about this.

2.4.2. Mean of sample-specific optimised parameterised transfer functions

As a result of the inherent randomness of ocean waves, and thus the seaway, it is unlikely that two identical operational situations, characterised by the exact same wave spectrum, speed, course, etc., lead to two exactly identical response spectra for the same measured response. In other words, although two sets of measurements of a given response (say, pitch) may be taken under seemingly identical conditions during two, say, 30-minutes periods, denoted by $\wp_1$ and $\wp_2$, it is not likely that the two corresponding optimised sets of parameters $\mathbf{Y}^*_{\wp_1}$ and $\mathbf{Y}^*_{\wp_2}$ will be exactly the same. To account for this randomness, an average value of the optimised parameters are computed, emphasising that the averaging is made element-wise, that is, separately for each element in $\mathbf{Y}$. This means that the final value is defined by,

$$\widetilde{\mathbf{Y}} = \text{mean}(\mathbf{Y}^*_{\wp}), \quad \forall\, \wp \tag{21}$$

where $\wp$ characterises any given time series sequence from which the parameterised transfer function has been optimised. In principle, the averaging could be made for *all* available data, as indicated by Eq. (21), with no account to the operational conditions, including sea state. On the other hand, it is reasonable to assume that $\mathbf{Y}$ shows dependency, notably, on significant wave height (reflecting a nonlinear relationship between wave and response) and relative wave direction (reflecting that the original, i.e. not-optimised, parameterised transfer function matches reality better for some encounter angles than others). In the numerical investigations in Sections 3 and 4 this discussion is continued.

As a practical remark, the derived "mean transfer function", as based on all sample-specific optimised parameterised transfer functions, is onwards referred to by *mean-optimised parameterised transfer function*, or just mean-optimised PTF.

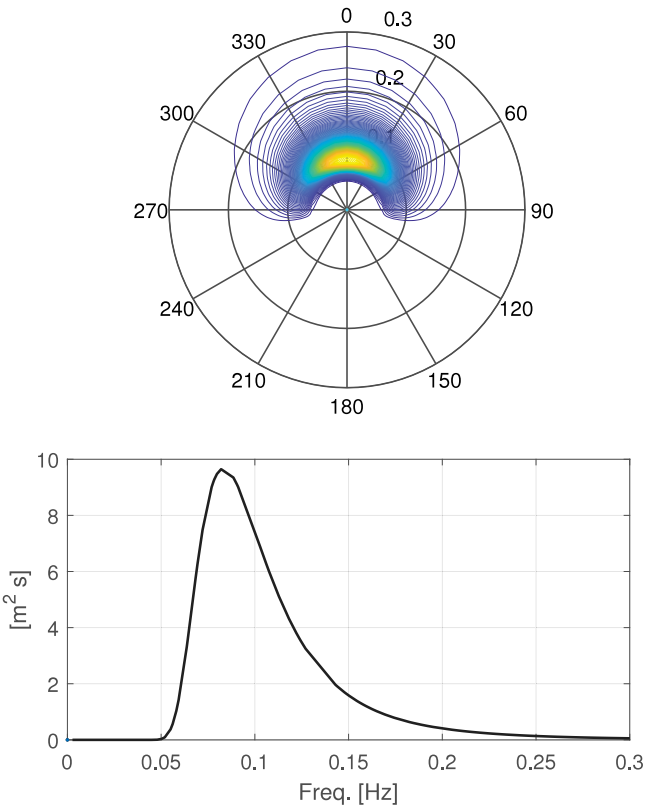

Fig. 2. Generating wave spectrum used for time series simulations. Note that the contour plot shows where the energy *comes* from.

2.5. Confidence bands

Confidence bands can be drawn around the predicted response spectrum as computed using the mean-optimised parameterised transfer function. The confidence bands would be obtained as the result of using all the different sample-specific sets $\mathbf{Y}^*_{\wp}$, $\wp = 1, 2, 3, \ldots, N_{\wp}$ to compute the transfer function; thus leading to $N_{\wp}$ indicative transfer functions, which all have (slightly) different dependency and behaviour with frequency in accordance with the formulas in Section 2.2. The results of all sample-specific optimised parameterised transfer functions at a given frequency can be used to compute the standard deviation of the transfer functions at that given frequency. In turn, this leads directly to the 95% confidence interval at the particular frequency, as this is obtained by, respectively, adding and subtracting two (1.96) standard deviations to/from the mean-optimised parameterised transfer function.

3. Case study based on simulated data

3.1. Ship data and time series simulations

A Ro-Ro vessel is studied. The specific vessel is characterised by main dimensions: Length L_{pp} = 232 m, breadth B = 33 m, draught T = 6.1 m, and block coefficient C_B = 0.61. The wave-to-motion transfer functions have been calculated by strip theory (Salvesen et al., 1970) for all six degrees of freedom, considering the whole range of wave encounter angles [0–360) deg., spaced by 10 deg., on a frequency interval [0.2–1.6] rad/s using 80 discrete, equidistantly spaced frequencies. The transfer functions have been computed for a speed U = 18 knots, equivalent to a Froude number F_n = 0.19. Later, it will be apparent that cases with following seas bring (expected) complexities resulting in poorer performance with the given settings. For this reason, it can be noted that the encounter frequencies, for which the triple-valued problem is a concern, i.e. when $\omega_e < \frac{1}{4\psi}$, are in the range 0.04 Hz ($\beta = 0$ deg) to infinity ($\beta = 89.9999$ deg).

Time series of the pitch motion have been simulated using the strip theory transfer function and a Bretschneider wave spectrum (e.g. Lloyd, 1998) assuming short-crested waves with a cos-2s spreading function, and vessel forward speed is 18 knots. The parameters used are: Significant wave height H_s = 3.0 m, peak period T_p = 12 s, spreading parameter s = 4. The wave spectrum is shown in Fig. 2. Simulations have been made for wave encounter angles $\beta = \{0, 10, 20, \ldots, 180\}$ deg., and for each encounter angle 10 time series, all with different seeds but with length 30 min, are simulated.

3.2. Results

This case study is used primarily to show that the sample-specific solution of the optimisation indeed varies, despite similar operational situations.

Arbitrarily selected outcomes (seed no. 3) of response spectra are shown in Fig. 3 considering different relative wave directions, as indicated by the title of the legend. In each plot, the measured spectrum $\widehat{S}_R(\omega_e)$ is shown together with three theoretical corresponding predictions $\widetilde{S}_{R,k}(\omega_e), k = 1,2,3$ obtained using the PTF in all cases: (1) the red curve (k = 1) is the spectrum based on the original PTF using the physical dimensions of the ship as input, (2) the cyan curve (k = 2) is the spectrum based on the sample-specific optimisation, (3) the blue curve (k = 3) is the spectrum based on the mean-optimised PTF, cf. Eq. (21), embracing all sample-specific optima in all wave directions. For each predicted spectrum, the legend presents the normalised summed-absolute error ϵ, computed using Eq. (17) relative to the area under the measured spectrum. Specifically, the error is defined by

$$\epsilon_k = \frac{\sum_{j=1}^{N_{\omega_e}} |\widetilde{S}_{R,k}(\omega_{e,j}) - \widehat{S}_R(\omega_{e,j})| \Delta\omega_e}{\widehat{m}_0} \cdot 100, \quad k = 1,2,3 \tag{22}$$

where N_{ω_e} is the number of discrete encounter frequencies spaced by the distance $\Delta\omega_e$. The multiplication with 100 [%] is made for convenience. Note that the denominator, i.e. the area under the measured spectrum represented by the zeroth moment $\widehat{m}_0$, is evaluated numerically by $\widehat{m}_0 = \int \widehat{S}_R(\omega_e) d\omega_e$.

Generally, the spectra computed from the sample-specific optimisation match very well with the measured spectra; in many cases with nearly exact matches between the measured and theoretically estimated results. The agreement reduces slightly when the mean-optimised PTF is used; notwithstanding, the agreement is significantly better compared to the case where the response spectra are obtained by use of the original PTF, based on the physical dimensions of the ship. An overall assessment can be seen in Fig. 4 that shows the statistics of the errors for each theoretical prediction using boxplots. On each box, the central mark indicates the median, and the bottom and top edges of the box indicate the 25th and 75th percentiles, respectively. The whiskers extend to the most extreme data points not considered outliers, and the outliers are plotted individually using the '+' symbol. It is seen that the improvement by the optimised PTF is only marginal for following sea cases (β = 0–50 deg). The reduced performance by the optimised PTF is a result of the computational complexities arising for spectral calculations in following sea (Beck et al., 1989; Lindgren et al., 1999), where very spiky spectra are obtained for the theoretical predictions, see Fig. 3. It is beyond the scope herein but improved results can most likely be obtained by using different settings related to the discretisation of the frequency vectors (encounter and absolute) in the spectral calculation, represented by Eq. (20). Although not shown herein, a few tests have been made in this direction. As will appear later, in Section 4, the problem with (very!) spiky theoretical spectra is also observed for the in-service data, and, for this case, a few alternative results are presented. Additional remarks will follow in Section 4, so the point left here to note is that a dedicated sensitivity study could possibly indicate how the frequency settings optimally could be made, depending on operational conditions.

Despite similar operational conditions, characterised by the same generating wave spectrum and even the same relative wave direction, the variation in the sample-specific optimised solution $\mathbf{Y}^*$ is large; as shown by Fig. 5. The figure shows the variation in the optimised values of the elements of $\mathbf{Y}^*$ using boxplots, similar to Fig. 4, and noticing that the first three elements are normalised. From this figure, in combination with the fact that the mean-optimised PTF is obtained by averaging over *all* available data, cf. Eq. (21), it can be easily explained why the use of the mean-optimised PTF does not produce as good results as the use of the sample-specific optimised PTF. The reason is simply that the variation in the parameters $\mathbf{Y}^*$ is significant, emphasising that some variation occurs even for cases when the relative wave direction is the same. It is interesting to note that the optimised values for $Y(1), Y(2), Y(3)$ are always smaller than the respective physical dimensions, corresponding to L, B, T, of the vessel. This is in agreement with the general observation that the original closed-form transfer functions (Jensen et al., 2004), for any given ship, always tend to drop to zero too early, when compared to other numerical codes such as strip theory or 3D panel codes. Another noteworthy point is that the solution of the optimisation, i.e. the values in $\mathbf{Y}^*$, are constrained with lower and upper bounds set as $0.5\mathbf{Y_0}$ and $1.25\mathbf{Y_0}$, respectively, where $Y_0(1) = L$, $Y_0(2) = B$, $Y_0(3) = T$, $Y_0(4) = 1$ are the initial guess and with L, B, T being the true physical main dimensions of the ship. The constraint is introduced for computational efficiency, and due to the fact that the original and non-optimised PTF (Jensen et al., 2004) qualitatively have proved to give consistent results. As a practical remark, it is observed that the lower bound, in some cases, is actually violated. This is an inherent problem of `fmincon`, which means that the function may occasionally produce values outside the specified range.[1] About the limitation to and below $1.0\mathbf{Y_0}$ for the physical dimensions (L,B,T) of the ship, this is a direct consequence of the fact that the original PTF by Jensen et al. (2004) yields a transfer function that drops to zero too early, as explained in the paper's introduction. Therefore, there is a need, in the optimisation, to reduce the vessel size to make the ship (more) responsive to higher frequency wave components. The exact reason why the maximum value is $1.0\mathbf{Y_0}$ is because this value is the starting guess of the optimisation, and, apparently, in some cases this leads to the optimal solution.

The actual parameter values corresponding to the mean-optimised PTF are the following: $\widetilde{Y}(1) = 208$ [m], $\widetilde{Y}(2) = 22.9$ [m], $\widetilde{Y}(3) = 5.13$ [m], and $\widetilde{Y}(4) = 1.06$. Hence, the mean-optimised PTF is computed by inserting $\widetilde{\mathbf{Y}}$ into the equations listed in Section 2.2 with $L = \widetilde{Y}(1)$, $B = \widetilde{Y}(2)$,

[1] Refer to https://se.mathworks.com/matlabcentral/answers/101965-why-are-the-upper-and-lower-bounds-violated-during-iterations-with-the-fmincon-function-from-the-opt.

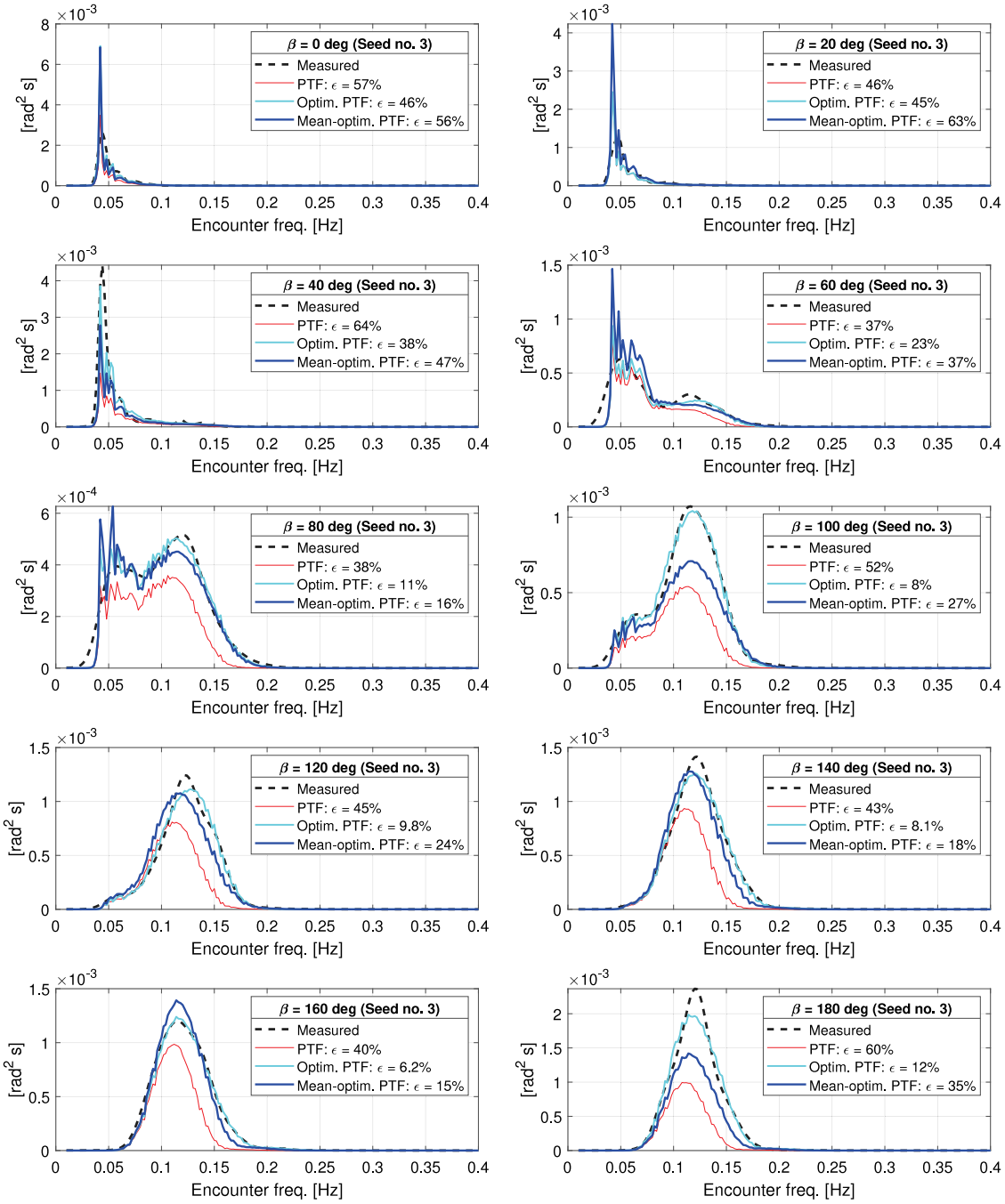

Fig. 3. Arbitrarily selected response spectra for relative wave directions {0, 20, 40, 60, 80, 100, 120, 140, 160, 180} deg; all taken from seed no. 3. The normalised error ϵ is included for each calculation using the parameterised transfer function (PTF). Note the difference in scale on the y-axis in the subplots.

$T = \widetilde{Y}(3)$, and $C_1 = \widetilde{Y}(4)$. In Fig. 6, the mean-optimised PTF is compared graphically to the solution of strip theory that, in this particular case with simulated data, represents the ground truth. The figure shows plots applicable to different relative wave directions, and in each plot the ground truth is shown as the full lines whereas the mean-optimised PTF is shown as the dashed lines. The result corresponding to the original PTF (Jensen et al., 2004) is also included in the plots as the thin dashed lines. It is appreciated that the mean-optimised PTF is a much better match to the ground truth than the original PTF. To this end, it appears relevant to stress that, although the strip theory transfer function of pitch can be regarded as the ground truth in the sense that it was used for the calculation of the time series simulation, the use of the strip theory transfer function itself will not reproduce the measured spectrum exactly in spectral calculations. The reason is that the measured spectrum, derived from time series simulations, also reflects the inherent randomness of the waves, and this randomness is not accounted for in spectral calculations based on the combination of a transfer function and a wave spectrum. This point is demonstrated in the plot in Fig. 8 which corresponds to the subplot in Fig. 3 for $\beta = 60$ deg. In Fig. 8, however, only the computed spectra obtained by use of the mean-optimised PTF and the "ground true" transfer function (from strip theory) are presented together with the measured spectrum.

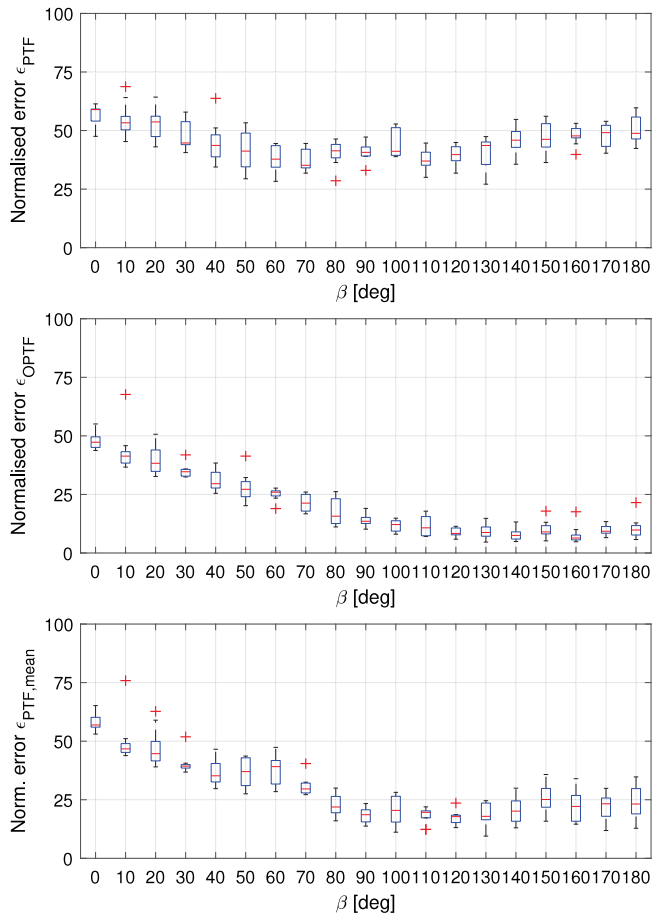

Fig. 4. Boxplot showing statistics of the normalised error between m_0 of the calculated and the measured response spectrum, cf. Eq. (22); the upper plot shows the error using the *original* (Jensen et al., 2004) parameterised transfer function (PTF), the middle plot shows the error using the sample-specific optimised PTF, the lower plot shows the error using the mean-optimised PTF.

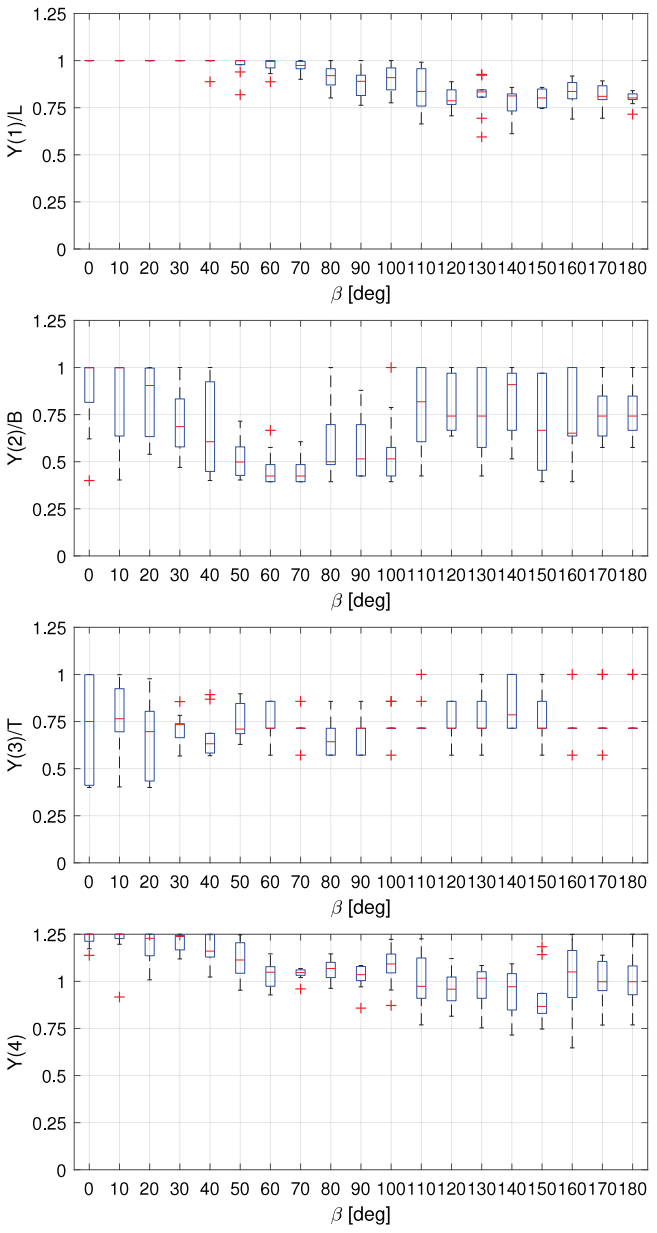

Fig. 5. Statistics of the optimised parameters $\mathbf{Y}^*$ shown via boxplots. Note that Y(1), Y(2), and Y(3) are normalised by their respective physical counterparts L, B, and T, respectively, whereas Y(4) = C_1.

It is observed that, in the given case, the use of the mean-optimised PTF, in fact, leads to the better prediction of the measured spectrum. Suffice it to mention that fairly similar results are obtained for the other relative wave directions and seeds with a somewhat equal performance by the mean-optimised PTF and strip theory, fluctuating between the one or the other as the better.

As suggested in Section 2.5, the variation between the sample-specific PTFs at the given frequencies can be used to associate confidence bands together with the mean-optimised PTF. In this event, the result is presented in Fig. 7 that shows both the mean-optimised PTF and the corresponding solution of strip theory, equivalently, the ground true transfer function. It is observed that the mean-optimised PTF and the associated 95% confidence bands match the ground truth well at the frequencies where most of the response occurs. Some discrepancies are observed in the higher frequency range, characterised by little to no response. Fig. 7 applies to four specific relative wave directions, i.e. $\beta = \{0, 50, 120, 170\}$ deg., but the results are similar for all remaining directions, considering the appearance of the 95% confidence bands. It should be noted that, consistent with a physical viewpoint, the derived confidence bands do not necessarily have a slope identical to the mean-optimised parameterised transfer function, since the confidence bands exhibit a dependency on frequency which, in turn, means that the thickness of the bounding interval between the upper band and the lower band varies with frequency. Following this point, it should be realised that deriving a 'mean transfer function' from the mean of all sample-specific transfer function at a given frequency is, on the other hand, considered physically inconsistent, since this potentially leads to a spurious frequency-dependency.

4. Application to in-service data with use of ERA5 2D wave spectra

4.1. Ship data and voyage

A 7200 TEU container vessel is considered, see Table 1.

The container ship is equipped with a motion sensor (XSENS, MTi-30-6A5G4), and the measurements of this study have been recorded in-service. Seven days of consecutive data were obtained while the ship followed an east-bound route across the Northern Pacific Ocean, with measurements from the Sea of Japan to the Graham Island in Canada, see map in Fig. 9, in the period of April 1st 2016 to April 7th 2016. The

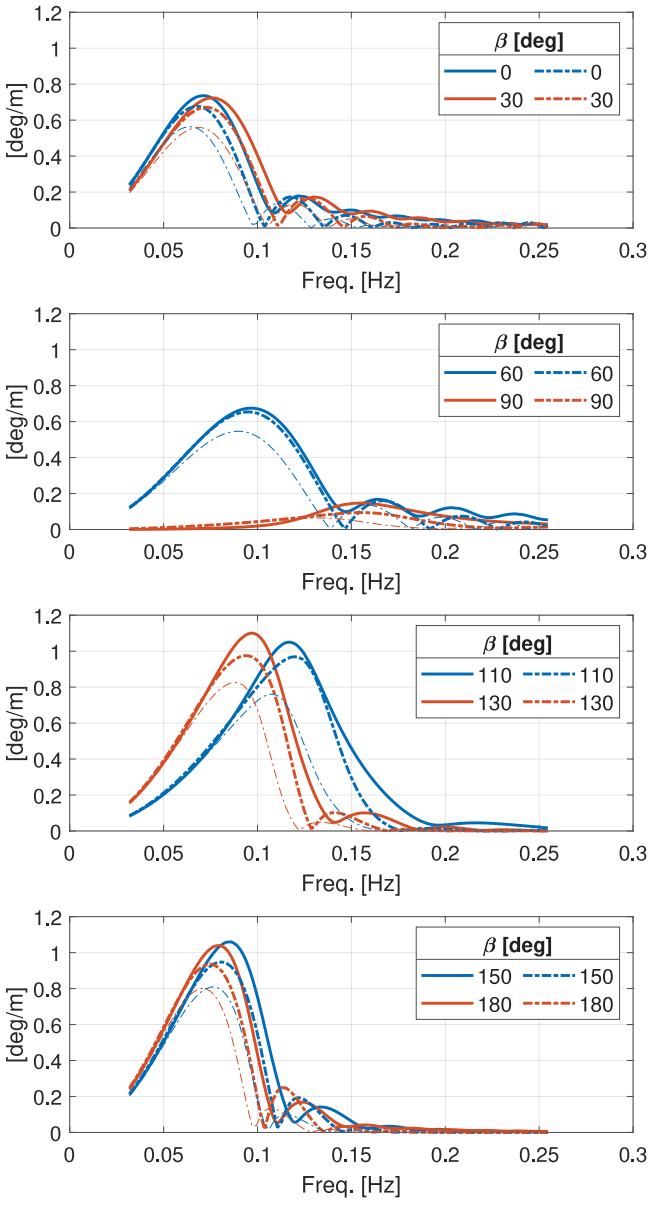

Fig. 6. Comparison between strip theory transfer function, equivalent to the ground true transfer function, (full line) of pitch and the corresponding mean-optimised PTF (dashed line) for different relative wave directions. Note that the original PTF (no optimisation) is included as the thin dashed line.

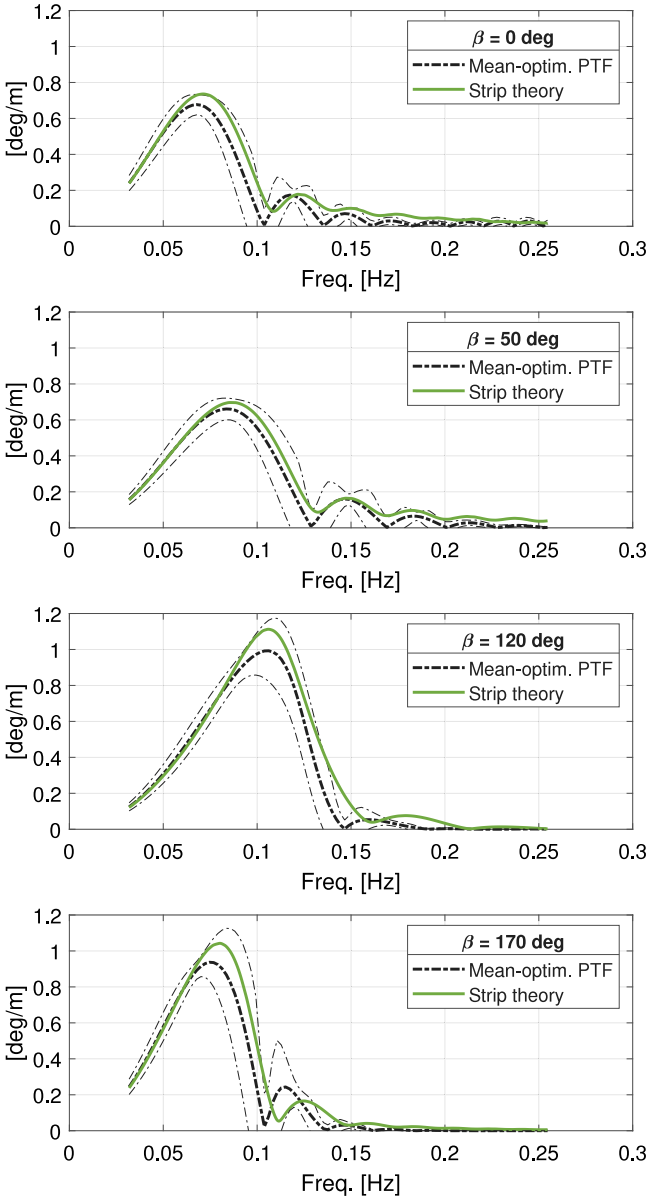

Fig. 7. Examples of mean-optimised PTF with associated 95% confidence bands compared with strip theory, equivalent to the ground truth. The plots apply for different relative wave directions as indicated by each legend.

Table 1
Main particulars of the example ship.

Length between perpendiculars, L_{pp}	332 m
Breadth moulded, B_m	42.8 m
Design draught, T_d	12.2 m
Deadweight (at T_d),	76,660 ton
Block coefficient, C_B	0.65

particular motion sensor was installed in a position off the centreline in the engine control room (Nielsen and Dietz, 2020b). In this study, focus is given to the measured pitch motion exclusively.

An overview of the operational conditions has been given by Nielsen and Dietz (2020b), suffice it here to mention that vessel speed was (nearly) constant and the variation in draught was insignificant over the voyage with the following values $U = 21$ knots and $T_M = 14.1$ m, respectively.

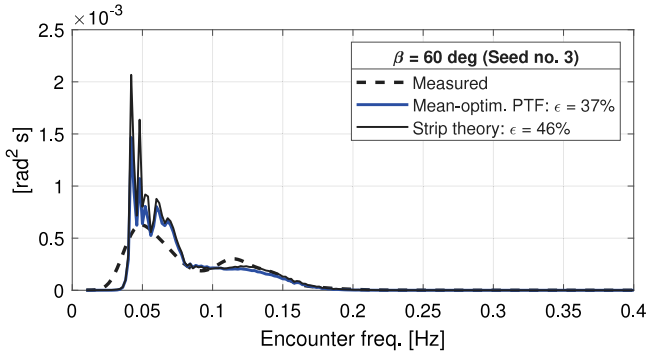

Fig. 8. Comparison of measured spectrum and corresponding theoretically computed spectra.

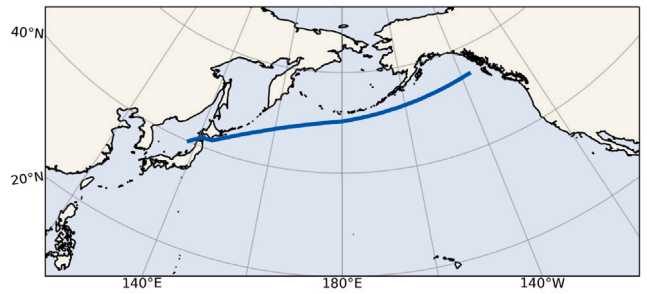

Fig. 9. Map of the east-bound voyage of the container ship across the Northern Pacific Ocean.

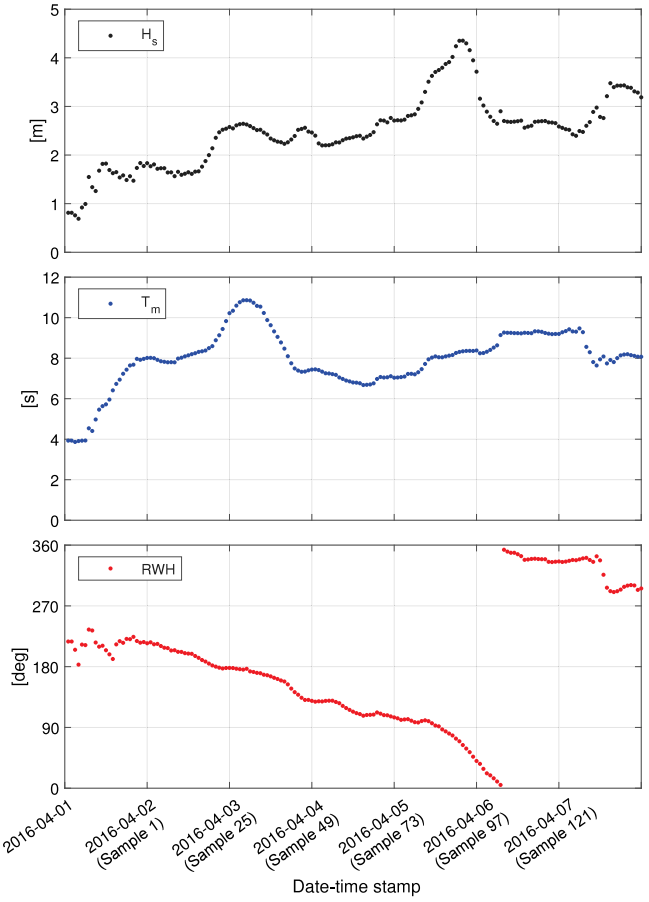

Fig. 10. Integral wave parameters at the nearest of the native ERA grid points at given date-time stamps in the format YYYY-MM-DD and indication of the corresponding sample numbering used later in the analysis. Top: significant wave height H_s; Middle: mean wave energy period T_m; Bottom: mean relative wave heading RWH (180 deg is head sea).

4.2. ERA5 wave spectra

The ERA5 dataset (Hersbach et al., 2021) provides hourly estimates of a large number of atmospheric, ocean-wave, and land-surface quantities on a discrete spatial grid, which for the ocean is spaced by 0.5 degrees in latitude and longitude. The reanalysis combines model data with satellite observations (ECMWF, 2017) – especially from the Copernicus EU-project (Copernicus Climate Change Service Information, 2020) – into a globally complete and consistent dataset.

In this study, the global-scale hourly ERA5 directional wave spectra, together with the associated sea state parameters, have been downloaded from Hersbach et al. (2021) using a routine in Python to cover the entire duration of the studied voyage, see Section 4.1. Each wave spectrum comprises components distributed in a frequency-direction grid, with 30 wave frequencies in the range [0.0345–0.5478] Hz and 24 circular directions spread evenly with a step of 15°. The available spectra which were located closest to the vessel's exact GPS position were selected for each time stamps in Coordinated Universal Time (UTC). A maximum distance of approximately 25 km has been observed between the ERA5 measurement point and the ship's position at the time stamp (Nielsen et al., 2021). The set of spectra obtained by this nearest-neighbour interpolation was considered as ground truth for the directional wave spectra near the ship's geographic position.

An overview of the encountered wave conditions during the voyage is presented in Fig. 10 via integral wave parameters, notably the significant wave height, the mean wave energy period, and the mean relative wave heading (RWH), emphasising that results apply to the nearest ERA5 grid point. The consequence of being off the native grid points has been investigated by Nielsen (2021) in a study focused on integral parameters, and it is concluded that it can be influential but generally the effect will be small. Anyhow, the present study uses the 2D wave spectra at the nearest ERA5 grid points in the analysis. As such, it is left to note that the mismatch in ship position and the nearest ERA5 grid point will introduce errors/uncertainties, but this issue is not considered herein. For interested readers, Nielsen and Dietz (2020a) provides a fairly complete overview of the encountered wave conditions, i.e. directional wave spectra; both those from ERA5 and those obtained using the ship as a wave buoy.

Returning to Fig. 10, it is interesting to note that the sea state is relatively low in the beginning of the voyage, the first day or so, with a small significant wave height and a low mean wave period. The low period means that waves with a short wave length, equivalently high frequency, characterise the wave systems. In *theory*, this means in turn that no substantial motions are induced, since the ship acts as a low-pass filter. As a result of this, it is decided to exclude the first 24 h of the data, so that the first sample considered in the analysis dates from 00:00 (UTC) on 2nd April. Thus, in total, 144 ($= 6 \times 24$) samples of measurement sequences are available for the optimising of the PTF.

4.3. Calculation of response spectra

Response spectra have been computed from 30-minutes time series sequences. The actual calculation is based on the estimated autocovariance function with frequency smoothing using a Parzen window function (Brodtkorb et al., 2000), and the resulting spectrum is low-pass filtered and interpolated to values at $f_e = (0.04 : 0.002 : 0.40)$ Hz, noting that $\omega_e = 2\pi f_e$. As mentioned in Section 4.2, the ERA5 2D wave spectra are updated on an hourly basis. Therefore, it is just every second response spectrum, equivalently pitch time series sequence, which is considered; noticing that the 30-minutes sequence is selected from a window starting and finishing 15 min prior to and succeeding, respectively, the corresponding hourly ERA5 update.

4.4. Results

The parameter values of the optimised vector $\mathbf{Y}^*$, as obtained for each of the 144 samples, are presented in Fig. 11. In line with the results for the simulated data, it is seen that $Y(1), Y(2), Y(3)$ in all cases take values smaller than or equal to their physical counterparts, being $L = 332$ m, $B = 42.8$ m, and $T = 12.2$ m, respectively. Likewise, relatively large variations can occur, even from the one sample to the following, in the single parameters. In this particular case, part of the variability of the optimal parameters can be attributed to the randomness of the encountered wave elevation sequence in similar operational conditions, and another part is a result of changes in the

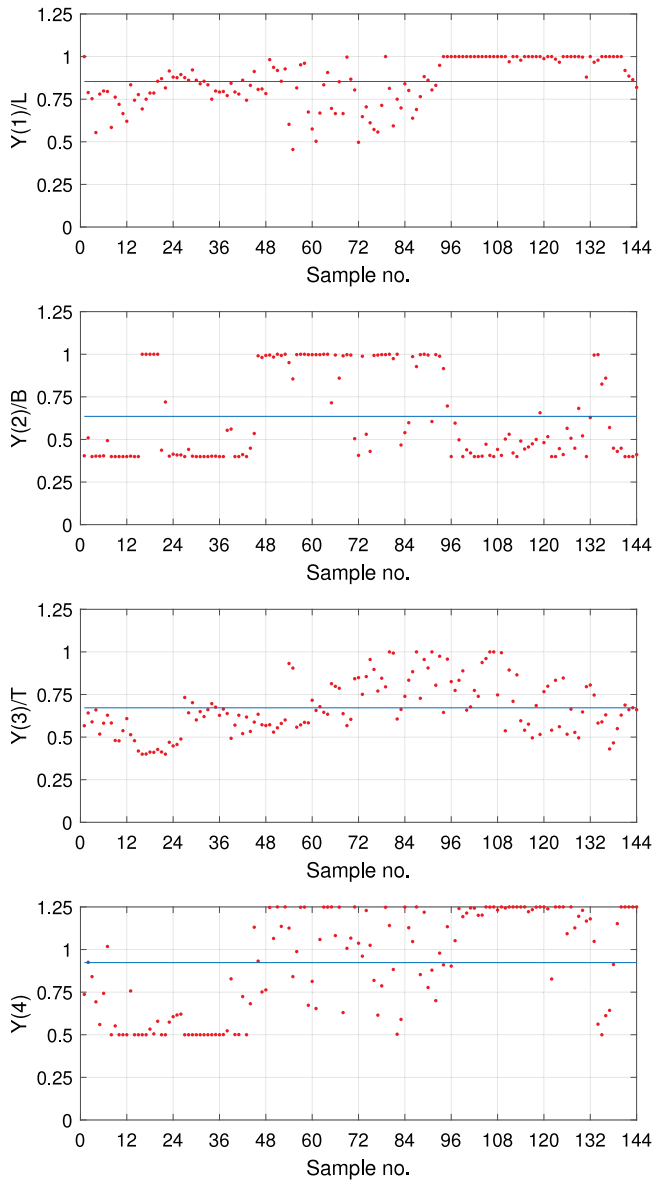

Fig. 11. Variation in the values of $\mathbf{Y}^*$ corresponding to the sample-specific optimisation for each of the 144 samples. Note that Y(1), Y(2), and Y(3) are normalised by their respective physical counterparts $L = 332$ m, $B = 42.8$ m, and $T = 12.2$ m, respectively, whereas $\mathrm{Y}(4) = C_1$. For each parameter, the mean value has been indicated with a thin blue line.

environmental conditions. For each parameter, the mean value based on all 144 samples is included as the thin blue line, and using the four respective mean values is what basically leads to the mean-optimised PTF. Further discussions about the use of the PTF follow below, but it is also interesting to see that, in the variability of the parameters, it can be argued that there are three main clusters: points from samples 1 to 44, then from sample 45 to 93, and finally from samples 94 to 144, where it is fair to say that the observation is a bit more evident for $Y(1)$ and $Y(2)$. As a suggested future work, this apparent clustering could be analysed by some Machine Learning method, and perhaps it could be used to find associations between the sea state parameters and the values of vector $\mathbf{Y}$.

Figs. 12 and 13 present results of response spectra for an arbitrarily selected set of samples. In each plot, corresponding to a given sample, the measured pitch spectrum is shown together with three theoretical computations: (1) The spectrum based on the sample-specific optimisation, referred to by 'Optim PTF', where the parameters in $\mathbf{Y}$ are optimised to yield a minimum error between the measured spectrum and the computed spectrum using the PTF. (2) The predicted spectrum based on the mean-optimised PTF. (3) The predicted spectrum based on a calculation using transfer functions computed by strip theory (Salvesen et al., 1970). It is observed that results of the original (non-optimised) PTF by Jensen et al. (2004) are *not* included in Figs. 12 and 13. This choice is intentional; first of all to limit the amount of information presented in the single plots. Secondly, the former study (Nielsen et al., 2021) did already present those results, which, to no surprise, were very poor. Returning to the theoretical predictions made in the present study, specifically with regards to (2), it should be noted that the mean-optimised PTF is derived in a similar manner as was explained in Section 3 studying simulated data. However, in this very case with in-service measurements, the data comprising the particular 20 samples in Figs. 12 and 13 has itself been excluded before the computation of the mean parameters $\widetilde{\mathbf{Y}}$, cf. Eq. (21). In this sense, to use Machine Learning terminology, the evaluation of the model, i.e. the mean-optimised PTF, is made using truly unseen data; this to replicate a real-case scenario, where the response is to be predicted solely on the basis of a model derived from past observations. In practice, on the other hand, it has an insignificant effect to include the very same samples (Figs. 12 and 13) in the "training data", since the method relies on computation of the mean values considering many samples. Here *many* is used to indicate that the mean values are computed using 144 samples taken from six days of measurements (cf. Fig. 11), or, alternatively, using 144-20 = 124 samples. In concrete numbers, by *ex*cluding the particular samples, the parameter values corresponding to the mean-optimised PTF become $\widetilde{Y}(1) = 266$ [m], $\widetilde{Y}(2) = 28.1$ [m], $\widetilde{Y}(3) = 9.54$ [m], and $\widetilde{Y}(4) = 0.82$, whereas the inclusion of the samples yield the following parameter values $\widetilde{Y}(1) = 269$ [m], $\widetilde{Y}(2) = 28.4$ [m], $\widetilde{Y}(3) = 9.56$ [m], and $\widetilde{Y}(4) = 0.83$. Hence, it means little to use the one set or the other set. It is noteworthy, however, that this observation holds only when an arbitrary set of samples is excluded.

This study is used to evaluate, on a conceptual level, the proposed method for determining transfer functions. As such, it is beyond the present scope to start discussing the exact details and the better, or worse, agreement for some samples of the shown response spectra in Figs. 12 and 13. Suffice it therefore to say that the spiky behaviour observed in the predictions for some samples, in line with results in Section 3, is a result of stern-quartering and/or following waves, and different frequency discretisation could therefore potentially lead to better results; see also Section 3 where a similar discussion was made on the basis of simulated data. Preliminary remarks in this regard are the following: The scales of the response spectra of, say, Samples 105, 111, 116, and 120 (Fig. 13) are inappropriate for a fair assessment. Zoomed versions of the particular spectra are shown in Fig. 14. While both predictions, i.e. the results of strip theory and the results of the mean-optimised PTF, including the sample-specific optimised PTF, are inconsistent with the measurements, the agreement between the predictions themselves is striking. It is believed that a dedicated sensitivity study could indicate if there would be an optimum setting of the discretisation of the frequency vector(s) used with Eq. (20). This type of work is beyond the present scope, but a few provisional results are seen in Fig. 15. The figure presents the response spectra of Samples 105, 111, 116, and 120, although results are shown only for the sample-specific optimised PTF, next to the measured spectra. In contrast to the results in Figs. 12 and 13, where the encounter frequency vector is discretised as $f_e = (0.04 : 0.002 : 0.40)$ Hz (cf. Section 4.3), the discrete values of the encounter frequency vector is $f_e = (0.04 : 0.005 : 0.40)$ Hz, and it is evident that the theoretical spectra – with a coarser frequency spacing – make up a better match to the measured spectra than seen in Fig. 13.

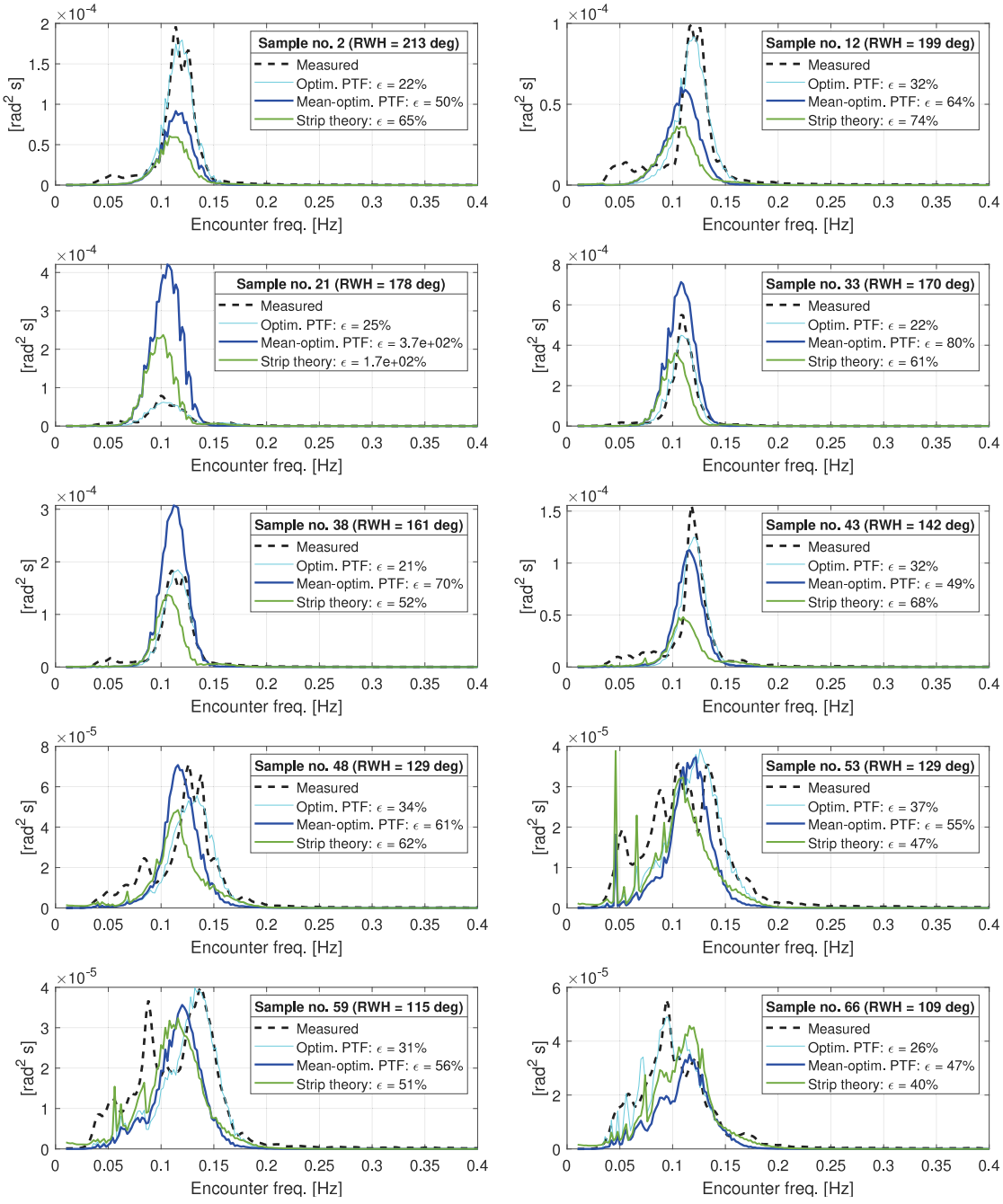

Fig. 12. Arbitrarily selected samples of response spectra. The mean relative wave heading (RWH) of the specific sample is included in the legend. [Continues in Fig. 13.].

The results, corresponding to what is achieved for the considered samples in Figs. 12 and 13, are representative. Hereby, it is understood that, considering other sets of samples, the results are generally similar for those samples; noting that the inclusion/exclusion of the particular samples before computing the mean parameters $\widetilde{\mathbf{Y}}$ by Eq. (21) is of little importance, as reported above. This observation, although not presented for other samples than those in Figs. 12 and 13, indicates that the proposed method for the computing of optimised parameterised transfer functions is fairly robust. A summary of the results is given in Fig. 16 that shows the normalised error, Eq. (22), using the sample-specific optimised PTF, the mean-optimised PTF, and the transfer function obtained by strip theory, respectively. In this case, the result corresponding to the mean-optimised PTF is simply based on *all* available data, i.e. all 144 samples taken from the six days. The main observation is that, overall, the use of the mean-optimised PTF yields results which agree well with the results obtained by using transfer functions computed with strip theory. The average error per sample has been calculated for the two (true) predictions,[2] and the result is included in the legend. It is seen that the average error is slightly smaller when using strip theory but it should also be noticed that the deviation is largely explained because of the discrepancy observed for Samples 12–30, where the use of the mean-optimised PTF produces too large response values. Otherwise, the two set of predictions exhibit the same trend and agree, as mentioned, nicely. Addressing the observation around Samples 12–30, it is somewhat

[2] Take note that the results from the sample-specific optimised PTF are not predictions as such.

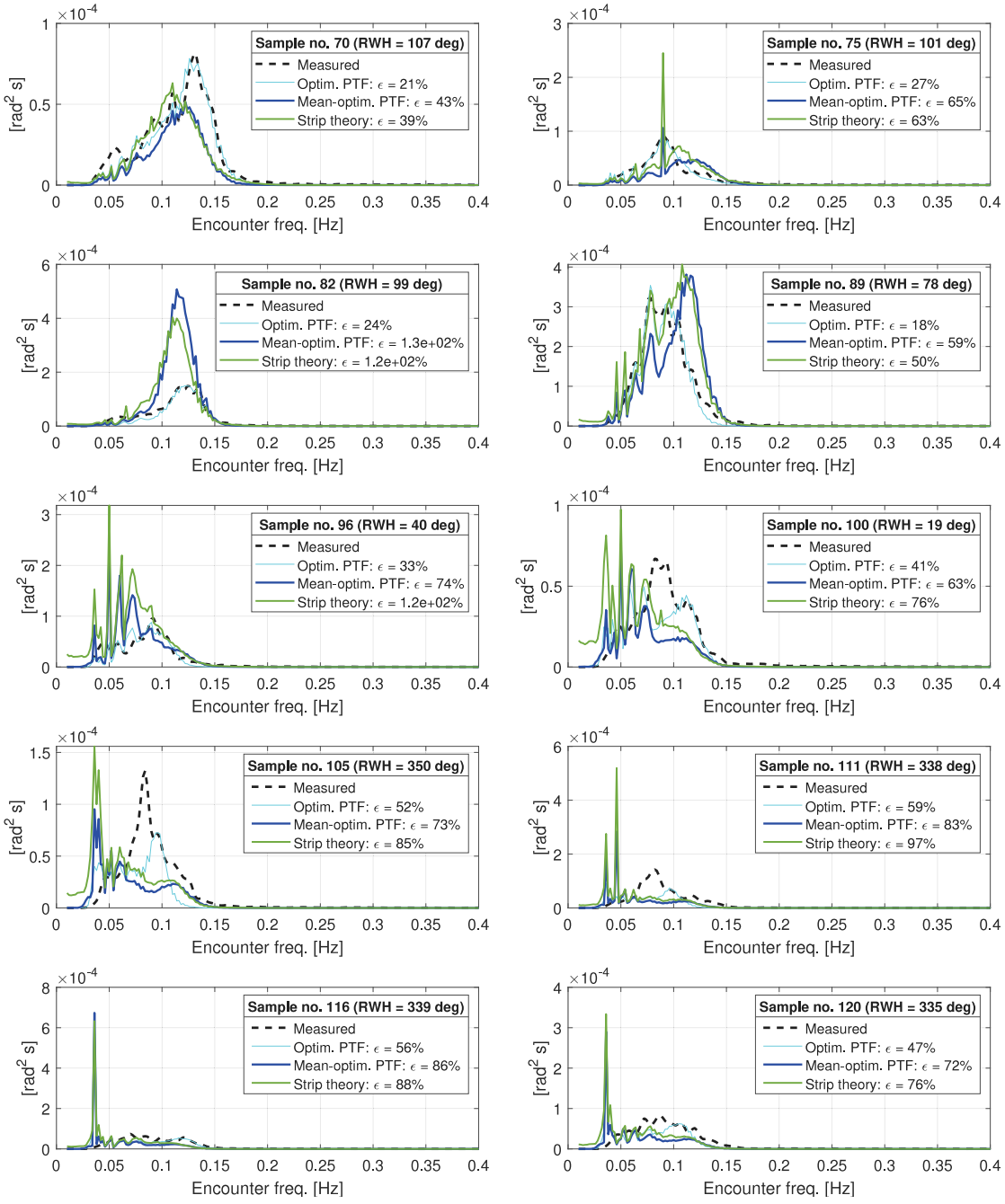

Fig. 13. [Continued from Fig. 12.] Arbitrarily selected samples of response spectra. The mean relative wave heading (RWH) of the specific sample is included in the legend.

peculiar to see the poor agreement for these cases, noting that poor(er) results are achieved by both strip theory and the mean-optimised PTF. The particular samples represent cases where the ship experiences bow-quartering and head waves. In this sense, it could be expected that predictions would perform relatively good, since the complexities in following sea are avoided, cf. Section 3. Speculations could be that the ERA5 directional wave spectra for the particular samples are not fully consistent with the ground truth, whatever this may be, thus leading to a mismatch between the theoretical predictions and the measurements. At the same time, it is possible that the mean-optimised PTF actually underperforms for head and bow-quartering waves, as indicated in the following.

The agreement between the mean-optimised PTF and the transfer functions from strip theory can be directly assessed by comparing the modula, and Fig. 17 presents the results for relative wave directions {0, 20, 40, …, 180} deg. The 95% confidence bands, cf. Section 2.5, of the mean-optimised PTF are included in all cases. Leaving aside the suspicious behaviour of the strip theory results for the higher frequency range in the following sea cases, overall there is a reasonable match between the mean-optimised PTF and the transfer function from strip theory. There is a tendency, however, that the mean-optimised PTF overshoots the peak and the response at the frequencies larger than the peak frequency for head sea cases, including bow-quartering waves. This tendency is likely what is observed from some of the samples of response spectra, where the spectrum computed from the mean-optimised PTF resulted in too large ordinates, see Fig. 12. In fact, this hypothesis is also supported by Fig. 10, which features bow-quartering to head sea condition for the particular samples.

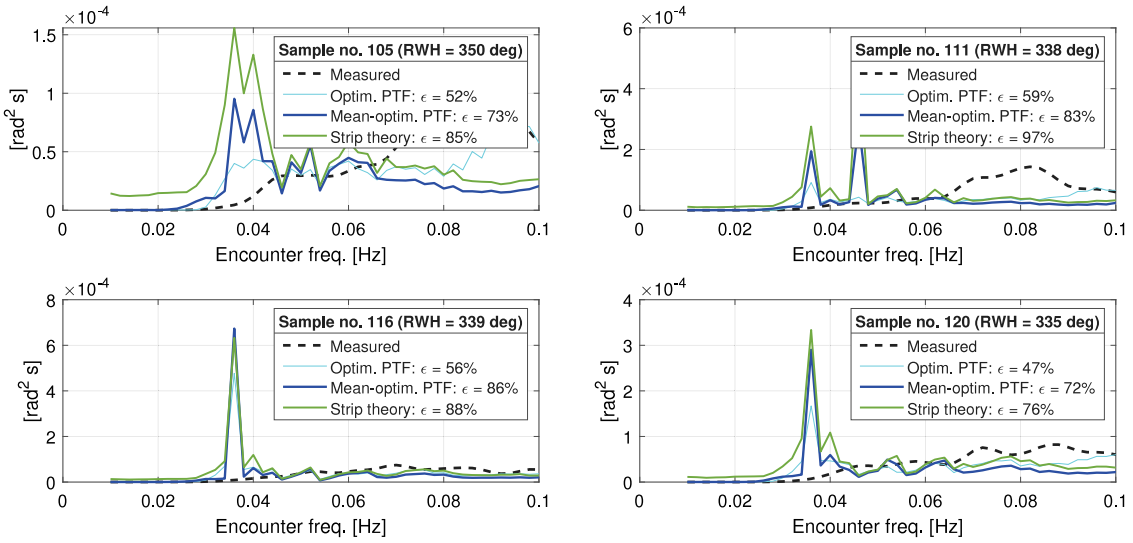

Fig. 14. Zoomed versions of the response spectra of Samples 105, 111, 116, and 120 which all represent cases with following waves.

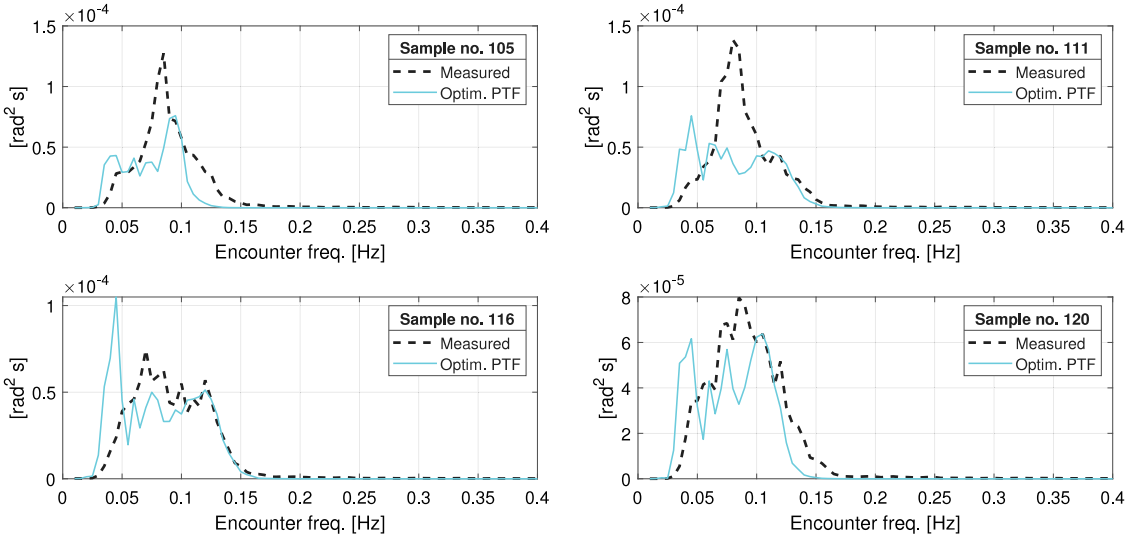

Fig. 15. Response spectra of Samples 105, 111, 116, and 120 using a different discretisation of the encounter frequency vector.

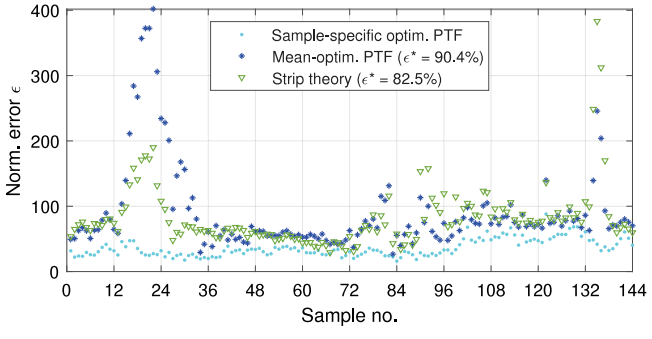

Fig. 16. Normalised error as computed by Eq. (22). The average error per sample, using the mean-optimised PTF and the strip theory transfer function, respectively, is included in the legend.

5. Additional discussions and future work

It should be realised that forward speed also has the potential to manipulate the shape of the transfer function. In fact, this has been investigated by Mounet et al. (2022a), where a sensitivity study using three different forward speeds is made in a work focused exclusively on simulated data. In the study, no explicit conclusions are drawn with respect to forward speed, in the sense that its inclusion as a tuning parameter does not really improve nor degrade the outcomes. As such, these observations are in line with initial investigations made at the beginning of the present study, where forward speed also was considered a fitting parameter, although those outcomes have not been mentioned or addressed. To follow this, herein it will not be attempted to make any firm conclusion towards the inclusion of forward speed, or not. This is said also because the inclusion of forward speed, as a fitting parameter, must be made by considering an additional choice: should the computation of the Doppler shift in connection with Eq. (20) also be made with forward speed as an optimising parameter. Future work

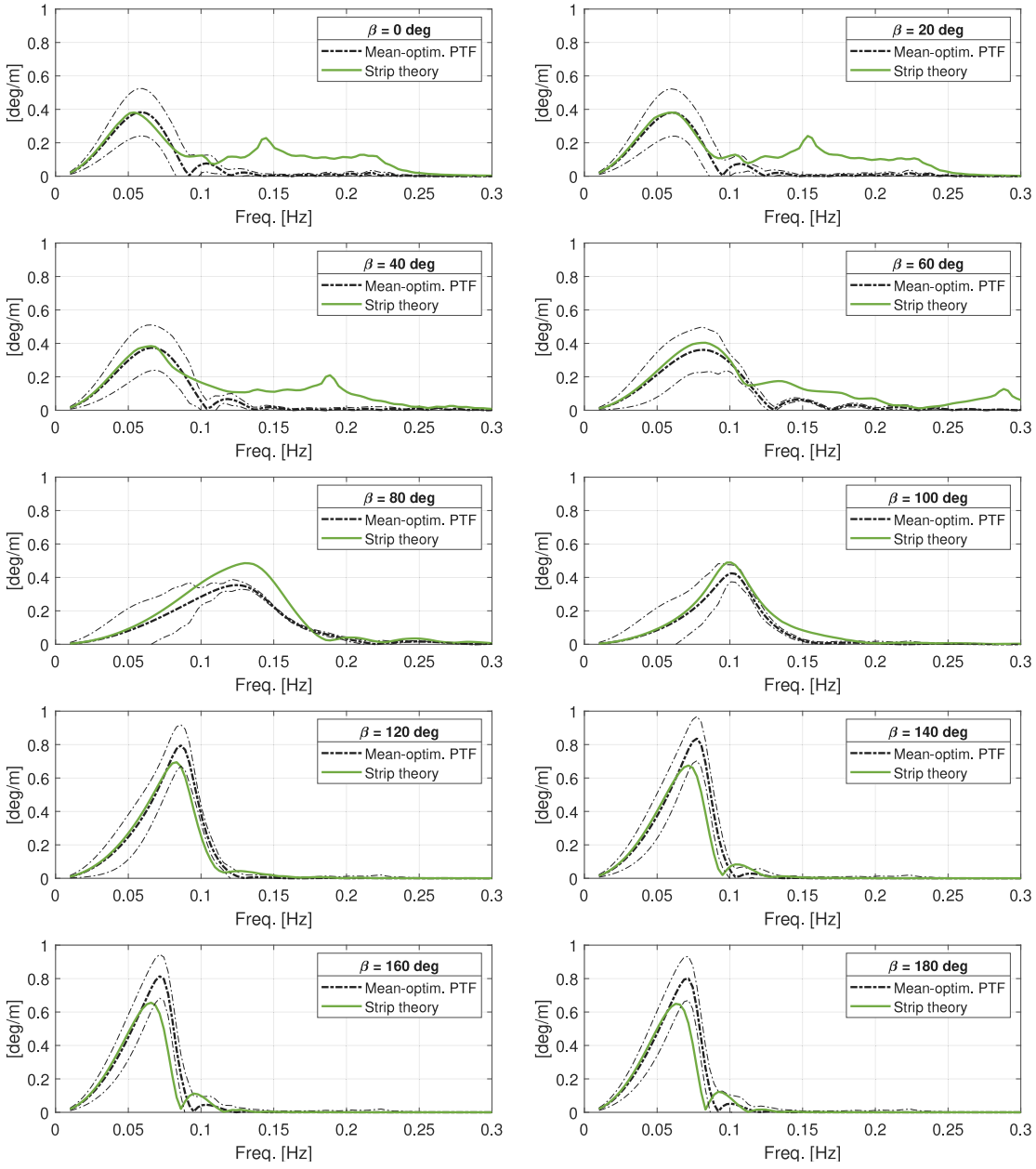

Fig. 17. Examples of mean-optimised PTF with associated 95% confidence bands. The plots apply for different relative wave directions as indicated by each legend.

could consider to take up this open question, especially considering the debate about the reliability of the speed log including the trustworthiness of position measurements derived from continuous monitoring systems (e.g. Ikonomakis et al., 2021, 2022).

The degree of variation in the sample-specific optimised parameters is a measure of the (un)certainty with which the *mean-optimised* PTF matches the ground truth; emphasising that the "ground truth" is a theoretical concept, since it has a true meaning only in case of simulation studies, whereas for real-data the ground truth is never known. As has been noticed, the sample-specific sets $\mathbf{Y}^*_{\wp}$, $\wp = 1, 2, 3, \ldots, N_{\wp}$ corresponding to consecutive samples of measurements can be quite different, despite fairly similar operational conditions from the one sample to the following. This was seen both for the case study using simulated data (Section 3) and from the results corresponding to in-service data (Section 4). Stated as a hypothesis, the less variation in $\mathbf{Y}^*_{\wp}$, $\wp = 1, 2, 3, \ldots, N_{\wp}$, the better a predictor is the mean $\widetilde{\mathbf{Y}}$ expected to be when applied together with unseen data. It is therefore suggested to associate a measure of uncertainty, based on the variation in the solution $\mathbf{Y}^*_{\wp}$ of the sample-specific optimisation. At this point, it is not clear how to consistently formulate such an uncertainty measure in a proper mathematical way but one possible measure could be expressed simply via the respective standard deviations observed in the single elements of $\mathbf{Y}^*_{\wp}$, relative to its mean value.

In the derived fashion, the confidence bands reflect uncertainties due to several phenomena: The inherent randomness in a wave elevation sequence (cf. the numerical case study using simulated data); the uncertainty in the "predicted" sea state (ERA5 is *not* the ground truth); the model uncertainty considering the fact that the optimised sample-specific PTF is not capable in mapping/matching perfectly the measured response spectrum in each and every case. It should be interesting to combine the aforementioned (potential) uncertainty measure with the confidence bands for the parameterised transfer function to better characterise the level of trust depending on operational conditions, sea state, frequency range, etc. In such an effort, it will be natural

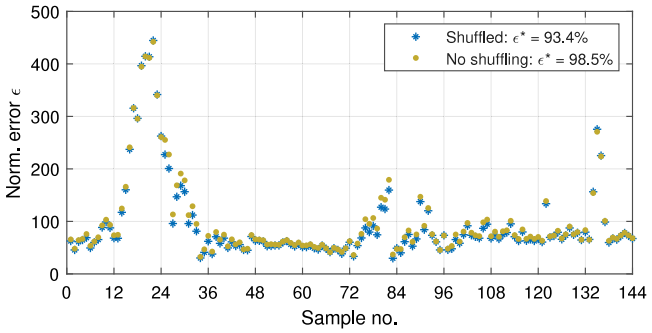

Fig. 18. Normalised error as computed by Eq. (22) based on six-fold cross validation with and without shuffling of the data. The average error per sample is included in the legend.

to make a more careful segmentation and selection of the "training data" than what has been made in the present conceptual evaluation. Next to being very comprehensive, however, it is also believed that any such future work requires a dataset much larger than the one studied herein. At this point, it seems relevant to make a note that Machine Learning very likely could be a helpful tool in not only the assessment of the results but also for the actual fitting of parameter values of the parameterised transfer functions.

The point made in the study is that the 95% confidence bands are indicative for a level of trust. On the other hand, it could also be interesting to directly apply the confidence bands in the prediction of response spectra for unseen data. This could, for instance, be done by computing the response spectrum based on the transfer function corresponding to both the upper band and the lower band, thus yielding two indicative response spectra that jointly form the prediction. Alternatively, but more computationally expensive, all sample-specific optimised transfer functions forming the training data could each and everyone be used to compute a whole set of response spectra that, on the frequency range, would form a "cloud" for the predicted response spectrum.

There are several different ways the data (i.e. the sample-specific optimised PTFs) can be split and/or sorted, and subsequently analysed. From a theoretical point of view, it is believed that it will be most sensible to sort the data according to sea state. This requires, as indicated previously, a lot more data than the present analysis is built on, since sufficiently many *different* sea states must have occurred; and preferably all of them more than once. An alternative to this is to set up a k-fold cross validation, which can be considered as a somewhat similar approach to what was actually done (cf. Figs. 12, 13, 16), although the conducted analysis in Section 4 was made with only one small part (approx. one sixth) of the data being unseen and constituting a validation set. Fig. 18 shows the outcome of a 6-fold cross validation, showing the outcome of only the mean-optimised PTF since the results of strip theory remains unchanged, and so does the sample-specific optimised PTF. In the figure, two sets of results are shown: One set where data is shuffled before validation, and another set without shuffling, thereby splitting the data in the precise order it was obtained to keep the chronology of the data. In either case, the six validation folds (comprising 24 unseen samples) have been concatenated to form the complete series. In this way, both sets of results yield the exact picture of how the method generalises to unseen data. The legend in the plot presents the average error per sample. From the analysis, it is evident that the outcomes are quite similar to the previous finding, cf. Fig. 16, and the associated observations remain. As a work left for the future, it could also be interesting to sort the data, and thus train, on the basis of the magnitude of the error obtained from the sample-specific optimised PTF.

The last point of the discussion is about the optimisation problem being solved. It seems quite reasonable to assume that the formulated nonlinear least squares problem is not necessarily convex, so the implemented algorithm (cf. Section 2.4.1) may very well find a local optimum; rather than the global one. It is definitely beyond the scope of the present study, but it could be interesting to see the effect of using a genetic algorithm, noticing that such ones are more computationally expensive but typically more suitable for finding the global optimum in nonlinear (non-convex) optimisation problems.

6. Concluding remarks

This paper presented a method from which to determine reliable transfer functions without the need of detailed hull geometry. Instead, the method relies on parameterised transfer functions (Jensen et al., 2004), and the availability of response measurements and associated wave conditions. The idea is based on the establishment of a cost function derived via spectral analysis equating the measured spectrum with the corresponding theoretically computed one using the parameterised transfer function and the wave spectrum. Solved as an optimisation problem, the solution yields the optimum set of parameters in the parameterised transfer function corresponding to a given measurement sample.

The study showed that the sample-specific optimum could vary quite much from one sample to the following. As a result, the mean values of the respective parameters of the sample-specific optima were computed by consideration of many samples. The achieved *mean-optimised* parameterised transfer function was associated with 95% confidence bands to indicate a level of trust depending on frequency.

Application on both simulated data and in-service measurements indicated promising results. Thus, reasonable agreement between the mean-optimised parameterised transfer function and the ground truth (simulated data), respectively, results obtained by strip theory (in-service measurements) was confirmed.

The main advantage of the presented method is considered to be its simplicity, repeating that the detailed hull geometry is not required. The simplicity comes with only a little price on accuracy, as compared to strip theory, but the small, if any, degradation is partly mitigated and/or compensated by the inclusion of the 95% confidence bands.

The fundamental assumption of the proposed method is that accurate 2D wave spectra are accessible. In the particular analysis of in-service measurements, the ERA5 dataset (Hersbach et al., 2020, 2021) was used. It is vital to stress that any ("consistent") inaccuracy or bias in the 2D wave spectra will be detrimental for the proposed method.

CRediT authorship contribution statement

Ulrik D. Nielsen: Conceptualization, Methodology, Software, Writing, Investigation, Visualization, Data provision, Discussion. **Raphaël E.G. Mounet:** Discussion, Writing – review & editing, Provision of ERA5 data, Visualization. **Astrid H. Brodtkorb:** Discussion, Writing – review & editing.

Declaration of competing interest

The authors declare that they have no known competing financial interests or personal relationships that could have appeared to influence the work reported in this paper.

Acknowledgements

The authors would like to thank Dr. Jesper Dietz (Maersk Line) in connection with data provision. The work has been supported by the Research Council of Norway through the Centres of Excellence funding scheme, project number 223254 AMOS. The second author is also financially supported by The Danish Maritime Fund, case numbers 2017-101 and 2020-074.

References

Beck, R., Cummins, W., Dalzell, J., Mandel, P., Webster, W., 1989. Vol. III: Motions in waves and controllability. In: Lewis, E. (Ed.), Principles of Naval Architecture, Second Revision. SNAME, Jersey City, NJ, USA, pp. 1–188.

Brodtkorb, P.A., Johannesson, P., Lindgren, G., Rychlik, I., Ryden, J., Sjö, E., Sköld, M., 2000. WAFO - A Matlab Toolbox for Analysis of Random Waves and Loads. Mathematical Statistics, Centre for Mathematical Sciences, Lund University, (The WAFO package can be downloaded freely on the internet).

Copernicus Climate Change Service Information, 2020. ERA5: Fifth generation of ECMWF atmospheric reanalyses of the global climate. https://cds.climate.copernicus.eu/cdsapp#!/home (accessed 08-01-2021).

ECMWF, 2017. Part VII: ECMWF Wave Model. Technical Report IFS Documentation – Cy43r3, European Center For Medium-Range Weather Forecasts, Shinfield Park, Reading, RG2 9AX, England.

Hersbach, et al., 2020. The ERA5 global reanalysis. Q. J. R. Meteorol. Soc. http://dx.doi.org/10.1002/qj.3803.

Hersbach, et al., 2021. ERA5 hourly data on single levels from 1979 to present. http://dx.doi.org/10.24381/cds.adbb2d47, https://cds.climate.copernicus.eu/cdsapp#!/dataset/reanalysis-era5-single-levels?tab=overview (accessed: 08-01-2021).

Ikonomakis, A., Nielsen, U., Holst, K., Dietz, J., Galeazzi, R., 2021. How good is the STW sensor? An account from a larger shipping company. J. Mar. Sci. Eng. 9, http://dx.doi.org/10.3390/jmse9050465.

Ikonomakis, A., Nielsen, U., Holst, K., Dietz, J., Galeazzi, R., 2022. Validation and correction of auto-logged position measurements. Commun. Transp. Res. 2, 100051.

Iseki, T., Ohtsu, K., 2000. Bayesian estimation of directional wave spectra based on ship motions. Control Eng. Pract. 8, 215–219.

Jensen, J.J., Mansour, A.E., Olsen, A.S., 2004. Estimation of ship motions using closed-form expressions. Ocean Eng. 31, 61–85.

Lindgren, G., Rychlik, I., Prevosto, M., 1999. Stochastic Doppler shift and encountered wave period distributions in Gaussian waves. Ocean Eng. 26, 507–518.

Lloyd, A.R.J.M., 1998. Seakeeping, second ed. Ellis Horwood.

Long, N., Sgarioto, D., Garratt, M., Sammut, K., Abbass, H., 2019. Multi-vessel sea state estimation utilising swarm shepherding. In: Proc. of IMC2019: Pacific International Maritime Conference. Sydney, Australia.

Mansour, A., Jensen, J., Olsen, A., 2004. Fast evaluation of the reliablity of container securing arrangements. In: Proceedings of PRADS'04. Travemünde, Germany. pp. 577–585.

Mounet, R.E.G., Nielsen, U.D., Brodtkorb, A.H., 2022a. A computationally efficient procedure for tuning of ship transfer functions. In: Proc. of 7th World Maritime Technology Conference. Copenhagen, Denmark.

Mounet, R.E.G., Nielsen, U.D., Brodtkorb, A.H., 2022b. Simultaneous sea state estimation and transfer function tuning using a network of dynamically positioned ships. Applied Ocean Research (under review).

Nielsen, U.D., 2006. Estimations of on-site directional wave spectra from measured ship responses. Mar. Struct. 19, 33–69.

Nielsen, U.D., 2017. Transformation of a wave energy spectrum from encounter to absolute domain when observing from an advancing ship. Appl. Ocean Res. 69, 160–172.

Nielsen, U., 2018. Deriving the absolute wave spectrum from an encountered distribution of wave energy spectral densities. Ocean Eng. 165, 194–208.

Nielsen, U.D., 2021. Spatio-temporal variation in sea state parameters along virtual ship route paths. J. Oper. Oceanogr. http://dx.doi.org/10.1080/1755876X.2021.1872894.

Nielsen, U.D., Brodtkorb, A., Sørensen, A., 2019. Sea state estimation using multiple ships simultaneously as sailing wave buoys. Appl. Ocean Res. 83, 65–76.

Nielsen, U.D., Dietz, J., 2020a. Estimation of sea state parameters by the wave buoy analogy with comparisons to third generation spectral wave models. Ocean Eng. 216, 107781.

Nielsen, U.D., Dietz, J., 2020b. Ocean wave spectrum estimation using measured vessel motions from an in-service container ship. Mar. Struct. 69, 102682.

Nielsen, U.D., Mounet, R.E.G., Brodtkorb, A.H., 2021. Tuning of transfer functions for analysis of wave - ship interactions. Mar. Struct. 79, 103029.

Parunov, J., Guedes Soares, C., Hirdaris, S., Iijima, K., Wang, X., Brizzolara, S., Qiu, W., Mikulic, A., Wang, S., Abdelwahab, H., 2022. Benchmark study of global linear wave loads on a container ship with forward speed. Mar. Struct. 84, 103162.

Salvesen, N., Tuck, E.O., Faltinsen, O., 1970. Ship motions and sea loads. Trans. SNAME 78, 250–287.

Yamamoto, Y., Sugai, K., Inoue, H., Yoshida, K., Fugino, M., Ohtsubu, H., 1986. Wave loads and response of ships and offshore structures from the viewpoint of hydroelasticity. In: Proceedings of the International Conference on Advances in Marine Structures. Admiralty Research Establishment, Dunfermline, Scotland.